Model of spin liquids with and without time-reversal symmetry

Jyong-Hao Chen,[1] Christopher Mudry,[1] Claudio Chamon,[2] and A. M. Tsvelik[3]
[1]*Condensed Matter Theory Group, Paul Scherrer Institute, CH-5232 Villigen PSI, Switzerland*
[2]*Department of Physics, Boston University, Boston, Massachusetts 02215, USA*
[3]*Condensed Matter Physics and Materials Science Division, Brookhaven National Laboratory, Upton, New York 11973-5000, USA*

(Received 11 November 2018; revised manuscript received 20 March 2019; published 30 May 2019)

We study a model in $(2+1)$-dimensional space-time that is realized by an array of chains, each of which realizes relativistic Majorana fields in $(1+1)$-dimensional space-time, coupled via current-current interactions. The model is shown to have a lattice realization as an array of coupled quantum spin-$1/2$ ladders. We study this model both in the presence and in the absence of time-reversal symmetry within a mean-field approximation. We find regimes in coupling space where Abelian and non-Abelian spin-liquid phases are stable. In the case when the Hamiltonian is time-reversal symmetric, we find regimes where gapped Abelian and non-Abelian chiral phases appear as a result of spontaneous breaking of time-reversal symmetry. These gapped phases are separated by a discontinuous phase transition. More interestingly, we find a regime for which a *nonchiral gapless non-Abelian* spin liquid is stable. The excitations in this regime are described by relativistic Majorana fields in $(2+1)$-dimensional space-time, much as those appearing in the Kitaev honeycomb model but here emerging in a model of coupled spin ladders that do not break the $SU(2)$ spin-rotation symmetry.

DOI: 10.1103/PhysRevB.99.184445

I. MOTIVATION AND SUMMARY OF RESULTS

The Kalmeyer-Laughlin chiral spin liquid [1] was the first example of a connection between the physics of the fractional quantum Hall (FQH) effect and that of frustrated quantum magnets that do not order through the spontaneous breaking of a symmetry. Such chiral spin liquids present exotic features, e.g., a ground-state degeneracy on the torus—a defining attribute of topological order [2]. The Kitaev honeycomb model [3] presents another example of a chiral spin liquid when a gap is opened by the addition of a magnetic field. The Kitaev model displays, in a regime of parameters, non-Abelian topological order, i.e., quasiparticles obey non-Abelian braiding statistics, as in the Moore-Read FQH states [4].

Recently, coupled-wire constructions pioneered by Kane and collaborators [5–9] have provided a complementary approach to the construction of topological ordered states, in particular, both Abelian and non-Abelian FQH states. These constructions allow one to utilize the powerful machinery of $(1+1)$-dimensional conformal field theory (CFT) to describe individual quantum wires at low energies, which are then coupled to their neighbors under periodic boundary conditions to gap the bulk degrees of freedom of the resulting two-dimensional system. Gapless chiral modes, described by chiral CFTs [10], are rather naturally obtained in these coupled-wire constructions under open boundary conditions.

Most of the focus of coupled-wire constructions has been on electronic systems with a quantized (charge) Hall response. However, one may also use, instead of quantum wires, quantum spin chains or ladders, which can also be described by CFTs in their gapless limits [11–16]. The result of these coupled-wire (i.e., coupled quantum spin-$1/2$ ladder) constructions are gapped chiral spin liquids in $(2+1)$-dimensional space-time [1,17], much as the electronic wire constructions lead to gapped FQH states.

Within this coupled-wire approach, we presented a model in Ref. [15] that, as we argued, displays chiral spin-liquid phases supporting both Abelian and non-Abelian topological orders. In that model, each quantum spin-$1/2$ ladder can be fine-tuned to a quantum critical point with a central charge of $c=2$. In turn, this quantum critical point can be thought of as the sum of four decoupled CFTs, each of which can be described by one flavor of a gapless Majorana field carrying the central charge $c=1/2$. These four independent Majorana fields per wire when fine-tuned to the $c=2$ quantum critical point can be arranged into a triplet and a singlet that transform like the spin one and spin zero representations of $SU(2)$, respectively. These Majorana fields are local within each wire so that quadratic terms, such as back-scattering are allowed *inside any given wire*. Back-scattering between the left- and the right-moving components of the singlet Majorana field is nothing but a singlet mass term m_{s}. It reduces the central charge $c=2$ to $c=3/2$. Equal amplitude back-scattering between the left- and the right-moving components of the triplet Majorana fields is nothing but a triplet mass term m_{t}. It reduces the central charge $c=2$ to $c=1/2$. Remarkably, the singlet and triplet masses [see Eq. (2.2)] realize a linear combination of local two- and four-body $SU(2)$ symmetric spin-$1/2$ interactions on a quantum spin-$1/2$ ladder (see Sec. IV). In this paper, we choose to fine-tune each wire (i.e., a quantum spin-$1/2$ ladder) to the $c=1/2$ quantum critical point that follows from gapping the triplet of Majorana fields. The question we then address is the effect of switching inter-wire interactions when each wire has been fine-tuned to its $c=1/2$ quantum critical point. Now, local interladder spin-$1/2$ interactions are *necessarily* quartic in the Majorana fields. They are characterized by a pair of dimensionless coupling

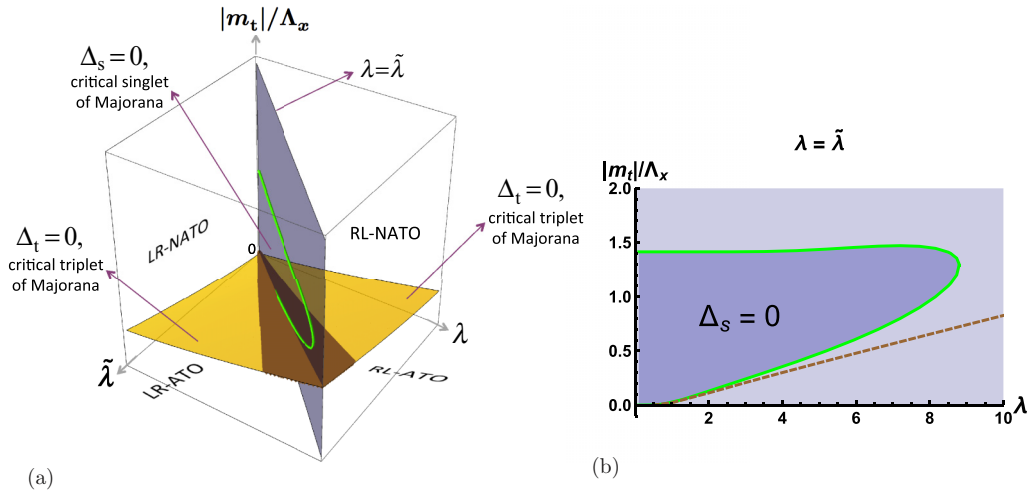

FIG. 1. (a) Mean-field phase diagram as a function of the three couplings $\lambda \geqslant 0$, $\widetilde{\lambda} \geqslant 0$, and $|m_t|/\Lambda_x$ for the theory defined in Eq. (2.4) under the assumptions (2.8) [Λ_x is a momentum cutoff that is introduced in Eq. (3.24b)]. The yellow surface represents those points in coupling space at which a continuous mean-field transition separates two distinct gapped phases of matter: an Abelian topological order (ATO) phase and a non-Abelian topological order (NATO) phase. The brown surface represents those points at which a *discontinuous* mean-field phase transition occurs. The acronym "LR" (respectively, "RL") refers to the chiralities of the gapless edge states, i.e., gapless edge states on the first wire m = 1 are left handed (respectively, right handed), whereas those on the last wire m = n are right handed (respectively, left handed) when open boundary conditions are chosen along the stacking direction of the wires. The quadrant $\lambda = \widetilde{\lambda}$ for which Hamiltonian density (2.4) is TRS is colored in gray. (b) For $|m_t/\Lambda_x| \geqslant 0$ and $\lambda = \widetilde{\lambda} \geqslant 0$, the region bounded by the vertical axis and the green colored continuous line supports a TRS mean-field solution as the minimum of the mean-field potential with the vanishing singlet gap $\Delta_s = 0$ and the nonvanishing triplet gap $\Delta_t = 2|m_t| \neq 0$ defined by Eq. (3.31). Outside of this region, TRS is spontaneously broken at the mean-field level with nonvanishing singlet $\Delta_s \neq 0$ and triplet $\Delta_t \neq 0$ gaps defined by Eq. (3.31). The brown dashed line is a line of discontinuous phase transitions that separates the mean-field snapshot of an ATO from a NATO phase.

constants λ and $\widetilde{\lambda}$ defined in Eq. (2.3) that are exchanged by the operation of time reversal. In Ref. [15], we studied the special case of $\lambda \neq 0$, $\widetilde{\lambda} = 0$ that maximally breaks time-reversal symmetry (TRS). This limit was analyzed using mean-field theory and a random-phase approximation that started from an exactly solvable limit. Within these approximations, we obtained the phase diagram of the coupled-ladder system with its gapped Abelian and non-Abelian chiral phases. The goal of this paper is to study the time-reversal symmetric limit $\lambda = \widetilde{\lambda}$ by exploring the zero-temperature phase diagram for arbitrary values of $\lambda \neq 0$, $\widetilde{\lambda} \neq 0$, and $|m_t| \geqslant 0$. The main results of this paper are summarized by the mean-field phase diagram presented in Fig. 1.

Summary of results: The phase diagram at zero temperature

In the present paper, intrawire interactions (i.e., spin-1/2 interactions in a single quantum spin-1/2 ladder that respect the $SU(2)$ spin-rotation symmetry) are parametrized by the dimensionful spin-singlet Majorana mass m_s and by the dimensionful spin-triplet Majorana mass m_t. Each wire is fine-tuned to the quantum critical point defined by the condition $m_s = 0$ in this parameter space. We then imagine switching adiabatically generic interwire interactions (i.e., generic $SU(2)$-symmetric interladder quantum spin-1/2 interactions) that are encoded by a pair of Majorana quartic interactions with the dimensionless couplings $\lambda \neq 0$ and $\widetilde{\lambda} \neq 0$. Because reversal of time exchanges $\lambda \neq 0$ and $\widetilde{\lambda} \neq 0$, the case of $\lambda \neq \widetilde{\lambda}$ breaks explicitly TRS, whereas the case of $\lambda = \widetilde{\lambda}$ is TRS. When TRS holds, the existence of *nonchiral* spin liquids becomes possible. Parameter space for the coupled wires is thus three dimensional. In Fig. 1, we choose the dimensionless couplings λ, $\widetilde{\lambda} \geqslant 0$, and $|m_t|/\Lambda_x$ where the momentum cutoff $\Lambda_x > 0$ is of the order of the band width of the spin excitations in the underlying quantum spin-1/2 ladder realizing a wire.

We find a rather rich phase diagram within a mean-field approximation, which we depict in Fig. 1. The mean-field phase diagram includes gapped phases of matter supporting gapless edge states that realize either $c = 2$ or $c = 1/2$ CFTs when open boundary conditions are imposed. By the bulk-edge correspondence, we infer that these mean-field gapped phases signal chiral Abelian and chiral non-Abelian topologically ordered quantum phases, respectively, when TRS is either explicitly or spontaneously broken. The logic connecting a mean-field phase diagram to a topologically ordered phase of quantum matter through the bulk-edge correspondence is very much the same as the one used by Read and Green [18] on the one hand hand and by Ivanov [19] on the other hand in their study of the braiding statistics of vortices in two-dimensional chiral p-wave superconductors.

In the case when TRS is spontaneously broken on the plane $\lambda = \widetilde{\lambda}$ of Fig. 1, we find that the Abelian and non-Abelian phases are separated by a *discontinuous mean-field quantum phase* transition. Although quantum phase transitions between distinct topological phases are often presumed to be continuous, we have discovered an example of a discontinuous phase transition at the mean-field level. Another example of discontinuous quantum phases transitions between topologically ordered phases of matter has been proposed for the Kitaev honeycomb model under a magnetic field within a

slave-particle mean-field theory and exact diagonalizations in Ref. [20].

More interestingly, we identify a region in the three-dimensional parameter space of Fig. 1 for which TRS remains unbroken. The region of Fig. 1 characterized by $\lambda = \widetilde{\lambda}$ with a vanishing mean-field singlet gap $\Delta_s = 0$ describes a gapless nonchiral spin liquid. In this region of parameter space, the Majorana fields acquire dispersion in the direction perpendicular to the ladders, yielding a pair of two-dimensional Majorana cones. We have, thus, found an example related to a quantum spin-1/2 lattice model in two-dimensional space with full $SU(2)$ spin-rotation invariance that supports a nonchiral spin-liquid phase with gapless Majoranas as in the phase B of the Kitaev honeycomb model [3]. However, $SU(2)$ spin-rotation symmetry is absent in the Kitaev honeycomb model. Now, realizing the Kitaev model requires a strong spin-orbit coupling [21,22], whereas our model does not. We have thus demonstrated by way of example that a gapless TRS spin-liquid phase does not require the breaking of spin-rotation symmetry. Keeping the $SU(2)$ spin-rotation symmetric interactions as the dominant ones may provide more opportunities in material science to realize quantum spin liquids experimentally [23].

The paper is organized as follows. We present the model of coupled Majorana fields and analyze several of its symmetries in Sec. II. We then study the model within a mean-field treatment in Sec. III. In Sec. IV, we discuss possible implications of this mean-field phase diagram for a lattice model of coupled spin-1/2 ladders that we propose as a regularization of the field theory defined in Sec. II. We summarize our results in Sec. V.

II. MODEL OF COUPLED MAJORANA FIELD THEORIES

A. Definition

Our quantum field theory (QFT) is built from four species (labeled by $\mu = 0, \ldots, 3$) of Majorana fields whose support is $(1+1)$-dimensional space-time. We will call this building block a ladder. This terminology is justified by the fact that we find in Sec. IV a quantum spin-1/2 ladder that regularizes this quantum field theory. We then consider n-independent copies of the Majorana quantum field theory in $(1+1)$-dimensional space-time with the kinetic Hamiltonian density,

$$\widehat{\mathcal{H}}_0 := \sum_{m=1}^{n}\sum_{\mu=0}^{3}\frac{i}{2}v_\mu\left(\widehat{\chi}^\mu_{L,m}\partial_x\widehat{\chi}^\mu_{L,m} - \widehat{\chi}^\mu_{R,m}\partial_x\widehat{\chi}^\mu_{R,m}\right), \tag{2.1a}$$

where the velocities v_μ are real valued and L, R denote the left and right movers, respectively. The Majorana fields $(\widehat{\chi}^\mu_{M,m})^* = \widehat{\chi}^\mu_{M,m}$ obey the equal-time anticommutators,

$$\left\{\widehat{\chi}^\mu_{M,m}(x), \widehat{\chi}^{\mu'}_{M',m'}(x')\right\} = \delta_{MM'}\delta_{mm'}\delta_{\mu\mu'}\delta(x-x'), \tag{2.1b}$$

with $\mu, \mu' = 0, \ldots 3$, $M, M' = L, R$, $m, m' = 1, \ldots, n$, and $0 \leqslant x \leqslant L_x$.

Besides the kinetic term (2.1a), we assume that there is a back-scattering term with real-valued couplings m_μ $(\mu = 0, \ldots, 3)$ inside each ladder,

$$\widehat{\mathcal{H}}_{\text{intraladder}} := \sum_{m=1}^{n}\sum_{\mu=0}^{3} i m_\mu \widehat{\chi}^\mu_{L,m}\widehat{\chi}^\mu_{R,m}. \tag{2.2}$$

We then couple consecutive ladders by considering interladder quartic interactions with real-valued coupling constants λ and $\widetilde{\lambda}$,

$$\widehat{\mathcal{H}}_{\text{interladder}} := \sum_{m=1}^{n-1}(\widehat{\mathcal{H}}_{\lambda,m} + \widehat{\mathcal{H}}_{\widetilde{\lambda},m}), \tag{2.3a}$$

$$\widehat{\mathcal{H}}_{\lambda,m} := \frac{\lambda}{4}\left(\sum_{\mu=0}^{3}\widehat{\chi}^\mu_{L,m}\widehat{\chi}^\mu_{R,m+1}\right)^2, \tag{2.3b}$$

$$\widehat{\mathcal{H}}_{\widetilde{\lambda},m} := \frac{\widetilde{\lambda}}{4}\left(\sum_{\mu=0}^{3}\widehat{\chi}^\mu_{R,m}\widehat{\chi}^\mu_{L,m+1}\right)^2. \tag{2.3c}$$

Each $\widehat{\mathcal{H}}_{\lambda,m}$ and $\widehat{\mathcal{H}}_{\widetilde{\lambda},m}$ term alone is the $O(4)$ Gross-Neveu-like quartic interaction.

The final Hamiltonian density is

$$\widehat{\mathcal{H}} := \widehat{\mathcal{H}}_0 + \widehat{\mathcal{H}}_{\text{intraladder}} + \widehat{\mathcal{H}}_{\text{interladder}}, \tag{2.4}$$

with $\widehat{\mathcal{H}}_0$, $\widehat{\mathcal{H}}_{\text{intraladder}}$, and $\widehat{\mathcal{H}}_{\text{interladder}}$ defined in Eqs. (2.1a), (2.2), and (2.3), respectively.

The limit $\widetilde{\lambda} = 0$ in the Hamiltonian density (2.4) was considered in Ref. [15]. This regime corresponds (with the singlet mass $m_s = 0$) to the planar region ($\lambda \geqslant 0$, $\widetilde{\lambda} = 0$, $m_t > 0$, $m_s = 0$) in Fig. 1 where ATO and NATO are the abbreviations for "Abelian topological order" and "non-Abelian topological order", respectively. A telltale to distinguish these phases is the central charge c of edge states: For Abelian phases, c is necessarily an integer; instead, if c is fractional, the phase is necessarily non-Abelian. (Note that it is possible to have integer c for non-Abelian phases, for instance, direct sums of models with fractional c's that add up to an integer.) In our model, the signatures of these phases at the mean-field level are the following. The edge states of a mean-field snapshot of the ATO phase are quadruplet of right-moving (left-moving) Majorana fermions $\widehat{\chi}^\mu_{R,1}$ ($\widehat{\chi}^\mu_{L,n}$) on the first (last) edge for $\mu = 0$–3, yielding $c = 4 \times 1/2 = 2 \in \mathbb{Z}$. The edge states of a mean-field snapshot of the NATO phase consist of the singlet Majorana modes $\widehat{\chi}^0_{R,1}$ and $\widehat{\chi}^0_{L,n}$ with $c = 1 \times 1/2 = 1/2 \notin \mathbb{Z}$.

The goal of this paper is to study the generic case where both λ and $\widetilde{\lambda}$ are *nonzero*. The phase diagram in Fig. 1 is mirror symmetric about the plane $\lambda = \widetilde{\lambda}$, and we will be particularly interested in the limit $\lambda = \widetilde{\lambda}$ at which the Hamiltonian density (2.4) is invariant under TRS.

B. Symmetries

Reversal of time is implemented by the m-resolved *antiunitary* $\mathbb{Z}_2$ transformation by which

$$\widehat{\chi}^\mu_{L,m}(x) \mapsto \widehat{\chi}^\mu_{R,m}(x), \tag{2.5a}$$

$$\widehat{\chi}^\mu_{R,m}(x) \mapsto \widehat{\chi}^\mu_{L,m}(x), \tag{2.5b}$$

$$i \mapsto -i \tag{2.5c}$$

for any $\mu = 0, \ldots, 3$, $m = 1, \ldots, n$, and $0 \leqslant x \leqslant L_x$.

The Hamiltonian density (2.4) has more symmetries. First, for arbitrary values of the masses and the couplings, the Hamiltonian density (2.4) is invariant under

$$\widehat{\chi}^{\mu}_{\mathrm{M,m}}(x) \mapsto \sigma^{\mu}\widehat{\chi}^{\mu}_{\mathrm{M,m}}(x), \quad \sigma^{\mu} = \pm 1 \tag{2.6}$$

for any $\mu = 0, \ldots, 3$, $\mathrm{M} = \mathrm{L}, \mathrm{R}$, $\mathrm{m} = 1, \ldots, n$, and $0 \leqslant x \leqslant L_x$. Second, it is also invariant under the m-resolved (local) $\mathbb{Z}_2$ transformation by which

$$\widehat{\chi}^{\mu}_{\mathrm{M,m}}(x) \mapsto \sigma_{\mathrm{m}}\widehat{\chi}^{\mu}_{\mathrm{M,m}}(x), \quad \sigma_{\mathrm{m}} = \pm 1 \tag{2.7}$$

for any $\mu = 0, \ldots, 3$, $\mathrm{M} = \mathrm{L}, \mathrm{R}$, $\mathrm{m} = 1, \ldots, n$, and $0 \leqslant x \leqslant L_x$.

Whenever the underlying lattice regularization of the Hamiltonian density (2.4) is endowed with a global $SU(2)$ symmetry, we will impose the conditions,

$$\begin{aligned} &v_0 \equiv v_{\mathrm{s}} \equiv v, \quad \mathrm{m}_0 \equiv m_{\mathrm{s}} = 0, \\ &v_a \equiv v_{\mathrm{t}} \equiv v, \quad \mathrm{m}_a \equiv m_{\mathrm{t}}, \quad a = 1\text{–}3, \end{aligned} \tag{2.8}$$

where s and t stand for singlet and triplet, respectively.

III. MEAN-FIELD APPROACH

A. Two auxiliary scalar fields

We will treat the interladder quartic interactions (2.3) by performing a Hubbard-Stratonovich transformation. To this end, we employ the Euclidean path-integral formalism and introduce two real-valued auxiliary scalar fields $\phi_{\mathrm{m,m+1}}$ and $\tilde{\phi}_{\mathrm{m,m+1}}$ for $\mathrm{m} = 1, \ldots, n-1$. The model (2.4) can then be written as

$$Z := \int \mathcal{D}[\phi, \tilde{\phi}] \int \mathcal{D}[\chi^0, \chi^1, \chi^2, \chi^3] e^{-S}, \tag{3.1a}$$

$$S := \int_0^{\beta} d\tau \int_0^{L_x} dx \sum_{\mathrm{m}=1}^{L_y/\mathfrak{a}_y} (\mathcal{L}_{\mathrm{f,m}} + \mathcal{L}_{\mathrm{b,m}} + \mathcal{L}_{\mathrm{fb,m}}), \tag{3.1b}$$

$$\begin{aligned} \mathcal{L}_{\mathrm{f,m}} := \frac{1}{2}\sum_{\mu=0}^{3} \big[&\chi^{\mu}_{\mathrm{L,m}}(\partial_\tau + i v_\mu \partial_x)\chi^{\mu}_{\mathrm{L,m}} \\ &+ \chi^{\mu}_{\mathrm{R,m}}(\partial_\tau - i v_\mu \partial_x)\chi^{\mu}_{\mathrm{R,m}}\big] + \sum_{\mu=0}^{3} \mathrm{i} m_\mu \chi^{\mu}_{\mathrm{L,m}}\chi^{\mu}_{\mathrm{R,m}}, \end{aligned} \tag{3.1c}$$

$$\mathcal{L}_{\mathrm{b,m}} := \frac{1}{4\lambda}(\phi_{\mathrm{m,m+1}})^2 + \frac{1}{4\tilde{\lambda}}(\tilde{\phi}_{\mathrm{m,m+1}})^2, \tag{3.1d}$$

$$\begin{aligned} \mathcal{L}_{\mathrm{fb,m}} := &\sum_{\mu=0}^{3} \frac{1}{2}\big(-i\chi^{\mu}_{\mathrm{L,m}}\chi^{\mu}_{\mathrm{R,m+1}}\big)\phi_{\mathrm{m,m+1}} \\ &+ \sum_{\mu=0}^{3} \frac{1}{2}\big(-i\chi^{\mu}_{\mathrm{R,m}}\chi^{\mu}_{\mathrm{L,m+1}}\big)\tilde{\phi}_{\mathrm{m,m+1}}. \end{aligned} \tag{3.1e}$$

Here, β is the inverse temperature and $\mathfrak{a}_y$ is the spacing between two consecutive ladders.

B. Symmetries

The action (3.1b) with $\lambda = \tilde{\lambda}$ is invariant under the m-resolved antiunitary time-reversal transformation [cf. Eq. (2.5)],

$$\begin{aligned} &\chi^{\mu}_{\mathrm{M,m}}(\tau, x) \mapsto \chi^{\mu}_{\mathrm{M',m}}(\tau, x), \quad \mathrm{M} \neq \mathrm{M}', \\ &\phi_{\mathrm{m,m+1}}(\tau, x) \mapsto -\tilde{\phi}_{\mathrm{m,m+1}}(\tau, x), \\ &\tilde{\phi}_{\mathrm{m,m+1}}(\tau, x) \mapsto -\phi_{\mathrm{m,m+1}}(\tau, x) \end{aligned} \tag{3.2}$$

for any $\mu = 0, \ldots, 3$, $\mathrm{M} = \mathrm{L}, \mathrm{R}$, $\mathrm{m} = 1, \ldots, n$, $0 \leqslant \tau \leqslant \beta$, and $0 \leqslant x \leqslant L_x$.

The action (3.1b) has the following additional symmetries. First, the μ-resolved Majorana parity is conserved owing to the symmetry of the action S (3.1b) under the $\mathbb{Z}_2$ transformation [cf. Eq. (2.6)],

$$\chi^{\mu}_{\mathrm{M,m}}(\tau, x) \mapsto \sigma^{\mu}\chi^{\mu}_{\mathrm{M,m}}(\tau, x), \quad \sigma^{\mu} = \pm 1 \tag{3.3}$$

for any $\mu = 0, \ldots, 3$, $\mathrm{M} = \mathrm{L}, \mathrm{R}$, $\mathrm{m} = 1, \ldots, n$, $0 \leqslant \tau \leqslant \beta$, and $0 \leqslant x \leqslant L_x$.

Second, the action (3.1b) is invariant under the m-resolved $\mathbb{Z}_2$ transformation [cf. Eq. (2.7)],

$$\begin{aligned} &\chi^{\mu}_{\mathrm{M,m}}(\tau, x) \mapsto \sigma_{\mathrm{m}}\chi^{\mu}_{\mathrm{M,m}}(\tau, x), \quad \sigma_{\mathrm{m}} = \pm 1, \\ &\phi_{\mathrm{m,m+1}}(\tau, x) \mapsto \sigma_{\mathrm{m}}\sigma_{\mathrm{m+1}}\phi_{\mathrm{m,m+1}}(\tau, x), \\ &\tilde{\phi}_{\mathrm{m,m+1}}(\tau, x) \mapsto \sigma_{\mathrm{m}}\sigma_{\mathrm{m+1}}\tilde{\phi}_{\mathrm{m,m+1}}(\tau, x) \end{aligned} \tag{3.4}$$

for any $\mu = 0, \ldots, 3$, $\mathrm{M} = \mathrm{L}, \mathrm{R}$, $\mathrm{m} = 1, \ldots, n$, $0 \leqslant \tau \leqslant \beta$, and $0 \leqslant x \leqslant L_x$.

C. Mean-field single-particle Hamiltonian

We do the mean-field approximation by which the Hubbard-Stratonovich fields ϕ and $\tilde{\phi}$ are assumed independent of the space-time coordinates (τ, x) and the ladder index m,

$$\phi_{\mathrm{m,m+1}}(\tau, x) \equiv \phi, \quad \tilde{\phi}_{\mathrm{m,m+1}}(\tau, x) \equiv \tilde{\phi}. \tag{3.5}$$

In what follows, we will ignore sign fluctuations of these Hubbard-Stratonovich fields ϕ and $\tilde{\phi}$ since as was demonstrated in Ref. [24] where fermions coupled to a $\mathbb{Z}_2$ gauge field on a square lattice were studied, such fluctuations are irrelevant. If so, the action from (3.1d) simplifies to

$$S_{\mathrm{b}} := \int_0^{\beta} d\tau \int_0^{L_x} dx \sum_{\mathrm{m}=1}^{L_y/\mathfrak{a}_y} \mathcal{L}_{\mathrm{b,m}} = \beta L_x \frac{L_y}{\mathfrak{a}_y}\left(\frac{1}{4\lambda}\phi^2 + \frac{1}{4\tilde{\lambda}}\tilde{\phi}^2\right). \tag{3.6}$$

We proceed by imposing periodic boundary condition along the y direction,

$$\chi^{\mu}_{\mathrm{M},n+1} \equiv \chi^{\mu}_{\mathrm{M},1} \tag{3.7}$$

for $\mathrm{M} = \mathrm{L}, \mathrm{R}$, and by performing the Fourier transformation,

$$\begin{aligned} S_{\mathrm{f}} + S_{\mathrm{fb}} &:= \int_0^{\beta} d\tau \int_0^{L_x} dx \sum_{\mathrm{m}=1}^{L_y/\mathfrak{a}_y} (\mathcal{L}_{\mathrm{f,m}} + \mathcal{L}_{\mathrm{fb,m}}) \\ &= \sum_{\omega,\boldsymbol{k}} \sum_{\mu=0}^{3} \frac{1}{2}\big(\chi^{\mu}_{-\omega,-\boldsymbol{k}}\big)^{\mathrm{T}}\big(i\omega\hat{\sigma}_0 + \widehat{H}^{\mathrm{MF}}_{\mu,\boldsymbol{k}}\big)\chi^{\mu}_{\omega,\boldsymbol{k}}, \end{aligned} \tag{3.8a}$$

where $\chi^{\mu}_{\omega,\boldsymbol{k}} := (\chi^{\mu}_{\mathrm{R},\omega,\boldsymbol{k}}, \chi^{\mu}_{\mathrm{L},\omega,\boldsymbol{k}})^{\mathsf{T}}$ for each flavor $\mu = 0, \ldots, 3$, the mean-field Majorana Hamiltonian is

$$\widehat{H}^{\mathrm{MF}}_{\mu,\boldsymbol{k}} := -v_\mu k_x \hat{\sigma}_3 - \Phi_+ \sin(k_y \mathfrak{a}_y)\hat{\sigma}_1 + [m_\mu - \Phi_- \cos(k_y \mathfrak{a}_y)]\hat{\sigma}_2, \tag{3.8b}$$

and we have introduced the linear combinations,

$$\Phi_\pm := \tfrac{1}{2}(\phi \pm \tilde{\phi}) \tag{3.8c}$$

for the auxiliary scalar fields. Here, $\hat{\sigma}_1$, $\hat{\sigma}_2$, and $\hat{\sigma}_3$ are Pauli matrices, whereas $\hat{\sigma}_0$ is the 2×2 identity matrix.

We can diagonalize the 2×2 single-particle Hamiltonian (3.8b) for each flavor $\mu = 0, \ldots, 3$. There follows eight branches of mean-field excitations with the dispersions (we have set $\mathfrak{a}_y = 1$),

$$\varepsilon_{\mu,\pm}(k_x, k_y) := \pm\varepsilon_\mu(k_x, k_y), \tag{3.9a}$$

$$\varepsilon_\mu(k_x, k_y) := \sqrt{v_\mu^2 k_x^2 + (m_\mu - \Phi_- \cos\, k_y)^2 + \Phi_+^2 \sin^2 k_y}. \tag{3.9b}$$

We see that the eight branches fall into four pairs of particle-hole symmetric bands. For an arbitrary value of k_x and k_y, the mean-field Majorana direct gap is defined by

$$\begin{aligned}\Delta_\mu(k_x, k_y) &:= \varepsilon_{+,\mu}(k_x, k_y) - \varepsilon_{-,\mu}(k_x, k_y) \\ &= 2\varepsilon_\mu(k_x, k_y).\end{aligned} \tag{3.10}$$

In the vicinity of $(k_x = 0,\ k_y = 0)$ and $(k_x = 0,\ k_y = \pi)$, the mean-field Majorana direct gaps are as follows:

$$\Delta_\mu(0, 0) = 2|m_\mu - \Phi_-| = 2\left|m_\mu - \frac{\phi}{2} + \frac{\tilde{\phi}}{2}\right|, \tag{3.11a}$$

and

$$\Delta_\mu(0, \pi) = 2|m_\mu + \Phi_-| = 2\left|m_\mu + \frac{\phi}{2} - \frac{\tilde{\phi}}{2}\right|, \tag{3.11b}$$

respectively. The minimum of the two gap functions (3.11) is

$$\Delta_\mu := 2\big||m_\mu| - |\Phi_-|\big| = 2\big||m_\mu| - \tfrac{1}{2}|\phi - \tilde{\phi}|\big|. \tag{3.12}$$

D. Linearized spectrum

The physics captured by the mean-field Majorana single-particle Hamiltonian (3.8b) becomes more transparent upon linearizing the latter around the gap closing points $(k_x, k_y) = (0, 0)$ and $(k_x, k_y) = (0, \pi/\mathfrak{a}_y)$, respectively. One finds the pair of 2×2 Dirac-like Hamiltonians,

$$\begin{aligned}&\widehat{H}^{\mathrm{MF}}_{\mu,k_x=0+p_x,\,k_y=0+p_y} \\ &\quad\approx -v_\mu p_x \hat{\sigma}_3 - \mathfrak{a}_y \Phi_+ p_y \hat{\sigma}_1 + (m_\mu - \Phi_-)\hat{\sigma}_2,\end{aligned} \tag{3.13a}$$

$$\begin{aligned}&\widehat{H}^{\mathrm{MF}}_{\mu,k_x=0+p_x,\,k_y=(\pi/\mathfrak{a}_y)+p_y} \\ &\quad\approx -v_\mu p_x \hat{\sigma}_3 + \mathfrak{a}_y \Phi_+ p_y \hat{\sigma}_1 + (m_\mu + \Phi_-)\hat{\sigma}_2.\end{aligned} \tag{3.13b}$$

Accordingly, $\mathfrak{a}_y\Phi_+$ plays the role of the Fermi velocity in the y direction. Furthermore, we find that the single-particle Majorana gap is $2|m_\mu \mp \Phi_-|$, in agreement with Eqs. (3.11a) and (3.11b). We now combine these linearized mean-field Majorana single-particle Hamiltonian into the 4×4 matrix,

$$\begin{aligned}\widehat{H}^{\mathrm{MF,lin}}_{\mu,\boldsymbol{p}} &:= \begin{pmatrix} \widehat{H}^{\mathrm{MF}}_{\mu,k_x=0+p_x,\,k_y=0+p_y} & 0_{2\times2} \\ 0_{2\times2} & \widehat{H}^{\mathrm{MF}}_{\mu,k_x=0+p_x,\,k_y=(\pi/\mathfrak{a}_y)+p_y} \end{pmatrix} \\ &= -v_{x,\mu} p_x \hat{\sigma}_3 \otimes \hat{\tau}_0 - v_y p_y \hat{\sigma}_1 \otimes \hat{\tau}_3 + m_\mu \hat{\sigma}_2 \otimes \hat{\tau}_0 \\ &\quad -\Phi_- \hat{\sigma}_2 \otimes \hat{\tau}_3,\end{aligned} \tag{3.14a}$$

where we have defined

$$v_{x,\mu} := v_\mu, \quad v_y := \mathfrak{a}_y \Phi_+, \tag{3.14b}$$

with the triplet $\hat{\tau}_1$, $\hat{\tau}_2$, and $\hat{\tau}_3$, a second set of Pauli matrices, and $\hat{\tau}_0$ as a second 2×2 identity matrix. This is an anisotropic single-particle Dirac Hamiltonian. The anisotropy enters through the two distinct Fermi velocities (3.14b) with the velocity along the y direction emerging from the nonvanishing value of Φ_+ for the bonding linear combination of the Hubbard-Stratonovich fields. There are two competing masses m_μ and the antibonding linear combination Φ_- of the Hubbard-Stratonovich fields that measures the amount by which the mean field breaks time-reversal symmetry. These masses compete because they multiply two 4×4 matrices that commute

$$[\hat{\sigma}_2 \otimes \hat{\tau}_0, \hat{\sigma}_2 \otimes \hat{\tau}_3] = 0. \tag{3.15}$$

The mass term $m_\mu \hat{\sigma}_2 \otimes \hat{\tau}_0$ breaks a unitary $\mathbb{Z}_2$ symmetry represented by conjugation with

$$\hat{\mathcal{I}} = \hat{\sigma}_3 \otimes \hat{\tau}_1. \tag{3.16}$$

The mass term $\Phi_- \hat{\sigma}_2 \otimes \hat{\tau}_3$ breaks time-reversal symmetry that is represented by conjugation with

$$\hat{\mathcal{T}} = \hat{\sigma}_1 \otimes \hat{\tau}_1 \mathsf{K}, \tag{3.17}$$

where K denotes the complex conjugation.

The competition between the mass terms $m_\mu \hat{\sigma}_2 \otimes \hat{\tau}_0$ and $\Phi_- \hat{\sigma}_2 \otimes \hat{\tau}_3$ implies a gap closing (i.e., continuous) transition when

$$|m_\mu| = |\Phi_-|, \tag{3.18}$$

that separates two single-particle insulating phases. As shown by Haldane [25], the Chern numbers for the pair of bands resolved by the flavor index μ is ± 1 when

$$|m_\mu| < |\Phi_-|. \tag{3.19}$$

This single-particle insulating phase realizes a Chern insulator at half-filling. When open boundary conditions are imposed, channel μ contributes one (Majorana) chiral edge state. The Chern numbers for the pair of bands resolved by the flavor index μ have vanishing Chern numbers when

$$|m_\mu| > |\Phi_-|. \tag{3.20}$$

This single-particle insulating phase is topologically trivial at half-filling. Gapless boundary states are not generic when open boundary conditions are imposed.

E. Mean-field potential

After integrating out the Majorana fields and expressing the scalar fields ϕ and $\tilde{\phi}$ in terms of $\Phi_\pm$ by using Eq. (3.8c), the

partition function (3.1) becomes

$$Z \propto \int \mathcal{D}[\Phi_+, \Phi_-] e^{-S_{\rm eff}}, \tag{3.21a}$$

where

$$S_{\rm eff} := S_{\rm B} + S_{\rm F}, \tag{3.21b}$$

$$S_{\rm B} := \frac{\beta L_x L_y}{\mathfrak{a}_y}\left[\frac{1}{4\lambda}(\Phi_+ + \Phi_-)^2 + \frac{1}{4\widetilde{\lambda}}(\Phi_+ - \Phi_-)^2\right], \tag{3.21c}$$

$$S_{\rm F} := -\frac{1}{2}\sum_{\mu=0}^{3}\sum_{\omega,\boldsymbol{k}} \ln\big[-\omega^2 - v_\mu^2 k_x^2 - (m_\mu - \Phi_- \cos\, q)^2 - \Phi_+^2 \sin^2 q\big], \tag{3.21d}$$

with $q := k_y \mathfrak{a}_y$.

When $\lambda = \widetilde{\lambda}$, the action (3.21) is invariant under a global antiunitary $\mathbb{Z}_2$ transformation defined by

$$\Phi_+ \mapsto -\Phi_+, \quad \Phi_- \mapsto \Phi_-, \quad \mathrm{i} \mapsto -\mathrm{i}. \tag{3.22}$$

This transformation is the mean-field counterpart to the time-reversal transformation defined in (3.3). We note that the μ-resolved global Majorana parity represented by the $\mathbb{Z}_2$ transformation (3.3) is invisible in the action (3.21) as we have integrated out Majorana fields. The m-resolved $\mathbb{Z}_2$ transformation (3.5) is also invisible in the action (3.21) since $\sigma_{\rm m} = \sigma_{\rm m+1}$ for any $\mathrm{m} = 1, \ldots, n$ under the mean-field approximation (3.5).

We are interested in the zero temperature and thermodynamic limit $\beta \to \infty$, $L_x \to \infty$, and $L_y \to \infty$ of the effective action (3.21). The summations then become integrals in three-dimensional space-time.

The Bosonic contribution to the mean-field potential is defined by

$$V_{\rm MF,B} := \frac{\mathfrak{a}_y}{\beta L_x L_y} S_B = \frac{1}{4\lambda}(\Phi_+ + \Phi_-)^2 + \frac{1}{4\widetilde{\lambda}}(\Phi_+ - \Phi_-)^2, \tag{3.23}$$

where S_B is given by Eq. (3.21c).

Similarly, the Fermionic contribution to the mean-field potential is

$$V_{\rm MF,F} := \frac{\mathfrak{a}_y}{\beta L_x L_y} S_{\rm F} := \sum_{\mu=0}^{3} V^{\mu}_{\rm eff,F}, \tag{3.24a}$$

where $S_{\rm F}$ is given by Eq. (3.21d) and we have defined

$$V^{\mu}_{\rm eff,F} := -\frac{1}{2}\int_{-\infty}^{+\infty}\frac{d\omega}{2\pi}\int_{-\Lambda_x}^{+\Lambda_x}\frac{dk_x}{2\pi}\int_{-\pi}^{+\pi}\frac{dq}{2\pi} \times \ln\big[\omega^2 + v_\mu^2 k_x^2 + (m_\mu - \Phi_- \cos\, q)^2 + \Phi_+^2 \sin^2 q\big], \tag{3.24b}$$

with Λ_x as a momentum cutoff that regularizes a divergent momentum integral over k_x. This momentum cutoff is on the order of the bandwidth for the spin excitations of the single quantum spin-1/2 ladder defined in Sec. IV that regularizes the quantum field theory describing a single wire. As it should be, the final expression for the mean-field potential (3.27) is independent of the value of Λ_x when the mean-field values of Φ_+ and Φ_- are measured in units of the momentum cutoff Λ_x. This is a typical feature of mean-field solutions in the (quasi-) one dimension [26].

After performing the integrals over the Matsubara frequency ω and over the momentum k_x [27],

$$\int_{-\infty}^{\infty}\frac{d\omega}{2\pi}\ln(\omega^2 + k^2 + A^2) = \sqrt{k^2 + A^2} + \text{const},$$

we are left with

$$V^{\mu}_{\rm eff,F} = -\Lambda_x^2 \frac{v_\mu}{4\pi}\int_{-\pi}^{+\pi}\frac{dq}{2\pi}\Big\{\sqrt{F_\mu^2(q)+1} + F_\mu^2(q)\ln\big[1 + \sqrt{F_\mu^2(q)+1}\big] - F_\mu^2(q)\ln\, F_\mu(q)\Big\}, \tag{3.25a}$$

where

$$F_\mu(q) := \frac{1}{v_\mu}\sqrt{\left(\frac{m_\mu}{\Lambda_x} - \frac{\Phi_-}{\Lambda_x}\cos\, q\right)^2 + \left(\frac{\Phi_+}{\Lambda_x}\right)^2 \sin^2 q}. \tag{3.25b}$$

Finally, the total mean-field potential $V_{\rm MF}$ is the addition of the bosonic mean-field potential $V_{\rm MF,B}$ (3.23) to the fermionic mean-field potential $V_{\rm MF,F}$ (3.24), i.e.,

$$V_{\rm MF} := V_{\rm MF,B} + V_{\rm MF,F}. \tag{3.26}$$

It is more convenient to rewrite $V_{\rm MF}$ (3.26) into the dimensionless form

$$v_{\rm MF}(\Phi_+, \Phi_-) := \Lambda_x^{-2} \times V_{\rm MF}(\Phi_+, \Phi_-) = \frac{1}{4\lambda}\left(\frac{\Phi_+}{\Lambda_x} + \frac{\Phi_-}{\Lambda_x}\right)^2 + \frac{1}{4\widetilde{\lambda}}\left(\frac{\Phi_+}{\Lambda_x} - \frac{\Phi_-}{\Lambda_x}\right)^2 - \frac{1}{4\pi}\sum_{\mu=0}^{3} v_\mu \int_{-\pi}^{+\pi}\frac{dq}{2\pi}\Big\{\sqrt{F_\mu^2(q)+1} + F_\mu^2(q) \times \ln[1 + \sqrt{F_\mu^2(q)+1}] - F_\mu^2(q)\ln\, F_\mu(q)\Big\}, \tag{3.27}$$

with $F_\mu(q)$ defined in Eq. (3.25b).

We observe that the mean-field potential (3.27) is invariant under

$$m_\mu \to -m_\mu, \quad \Phi_+ \to -\Phi_+, \quad \Phi_- \to -\Phi_-. \tag{3.28}$$

Thus, without loss of generality, we will assume that $m_\mu, \Phi_+ \geqslant 0$, whereas $\Phi_- \in \mathbb{R}$.

F. Saddle-point equations

The saddle-point equations stem from the first-order derivative of V_{eff} (3.27) with respect to Φ_+ and Φ_-, respectively,

$$0 = \left(\frac{1}{2\lambda} + \frac{1}{2\widetilde{\lambda}}\right)\Phi_+ + \left(\frac{1}{2\lambda} - \frac{1}{2\widetilde{\lambda}}\right)\Phi_- - \frac{1}{2\pi} \times \sum_{\mu=0}^{3}\left[\frac{1}{v_\mu}\int_{-\pi}^{+\pi}\frac{dq}{2\pi}\Phi_+ \sin^2 q \,\text{arcsinh}\left(\frac{1}{F_\mu(q)}\right)\right], \tag{3.29a}$$

$$0 = \left(\frac{1}{2\lambda} - \frac{1}{2\widetilde{\lambda}}\right)\Phi_+ + \left(\frac{1}{2\lambda} + \frac{1}{2\widetilde{\lambda}}\right)\Phi_- - \frac{1}{2\pi}\sum_{\mu=0}^{3} \times\left[\frac{1}{v_\mu}\int_{-\pi}^{+\pi}\frac{dq}{2\pi}(\Phi_- \cos q - m_\mu)\cos q \,\text{arcsinh}\left(\frac{1}{F_\mu(q)}\right)\right], \tag{3.29b}$$

where $F_\mu(q)$ is defined in Eq. (3.25b).

For simplicity, we assume a hidden $SU(2)$ symmetry that implies that the conditions (2.8) must hold (see Sec. IV). For simplicity, $v_{\text{s}} = v_{\text{t}} \equiv v \equiv 1$. We also assume that $m_{\text{s}} = 0$, a consequence of fine-tuning at a quantum critical point of a microscopic building block of the model (see Sec. IV A). We solve for (Φ_+, Φ_-) in Eq. (3.29) numerically for an arbitrary value of λ, $\widetilde{\lambda}$, and $\frac{m_{\text{t}}}{\Lambda_x}$. As we are only interested in local minima of the saddle-point equations (3.29), we use the Hessian matrix,

$$\mathbb{H}_{\text{Hess}} := \begin{pmatrix} \frac{\partial^2 V_{\text{MF}}}{\partial \Phi_+^2} & \frac{\partial^2 V_{\text{MF}}}{\partial \Phi_+ \partial \Phi_-} \\ \frac{\partial^2 V_{\text{MF}}}{\partial \Phi_- \partial \Phi_+} & \frac{\partial^2 V_{\text{MF}}}{\partial \Phi_-^2} \end{pmatrix}, \tag{3.30}$$

and demand that it is positive definite. A solution (Φ_+, Φ_-) of Eq. (3.29) is stable if the Hessian matrix evaluated at (Φ_+, Φ_-) is positive definite.

G. Mean-field phase diagram

By combining Eq. (2.8) with Eq. (3.12), we find the singlet and triplet gaps,

$$\Delta_{\text{s}} := 2|\Phi_-| = |\phi - \tilde{\phi}|, \tag{3.31a}$$

$$\Delta_{\text{t}} := 2\big||m_{\text{t}}| - |\Phi_-|\big| = 2\big||m_{\text{t}}| - \tfrac{1}{2}|\phi - \tilde{\phi}|\big|, \tag{3.31b}$$

respectively, given a stable solution (Φ_+, Φ_-) to the saddle-point equations (3.29). Correspondingly, we enumerate the following four possibilities:

$$\Phi_+ = +\Phi_- = +\phi/2 \neq 0, \quad \tilde{\phi} = 0, \tag{3.32a}$$

$$\Phi_+ = -\Phi_- = -\tilde{\phi}/2 \neq 0, \quad \phi = 0, \tag{3.32b}$$

$$\Phi_+ = \phi = \tilde{\phi}, \quad \Phi_- = 0, \tag{3.32c}$$

$$\Phi_- = (\phi - \tilde{\phi})/2 = \pm m_{\text{t}} \neq 0. \tag{3.32d}$$

Case (3.32a) is obtained when $\lambda > 0$ whereas $\widetilde{\lambda} = 0$. Case (3.32b) is obtained when $\lambda = 0$, whereas $\widetilde{\lambda} \neq 0$. Case (3.32c) implies that the singlet gap vanishes $\Delta_{\text{s}} = 0$, whereas the triplet gap is solely controlled by the triplet mass $\Delta_{\text{t}} = |m_{\text{t}}|$. Case (3.32d) implies that the triplet gap vanishes $\Delta_{\text{t}} = 0$, whereas the singlet gap is solely controlled by the triplet mass $\Delta_{\text{s}} \neq 2|m_{\text{t}}|$.

Figure 1 summarizes the numerical search for the stable solutions to the saddle-point equations (3.29) in the three-dimensional coupling space $\lambda \geqslant 0$, $\widetilde{\lambda} \geqslant 0$, and $|m_{\text{t}}| \geqslant 0$, holding v_μ and m_{s} fixed to the values $v_\mu \equiv 1$ and $m_{\text{s}} = 0$, respectively. The terminology ATO for Abelian topological order and NATO for non-Abelian topological order applies whenever the stable saddle point delivers Chern insulating bands with four and one chiral Majorana edge states, respectively, upon imposing the open boundary condition along the y direction. Which chirality is to be found on the left (m = 1) or right (m = n) ends of the model defined in Eq. (2.4) is specified by the combination of letters LR or RL. Of course, there is no topological order at the mean-field level as the ground state is nondegenerate when periodic boundary conditions are imposed. However, we conjecture that the ground-state manifolds in the ATO and NATO phases acquire distinct nontrivial topological degeneracies when the mean-field approximation is relaxed. Computing explicitly these topological degeneracies is beyond the scope of this paper. Nevertheless, the existence of bulk topological excitations can be inferred by invoking the bulk-edge correspondence—the chiral central charge of the CFT on the edge must be related to the unitary braided fusion category of the topological quantum field theory in the bulk (see Refs. [3,28,29]).

1. *Phase transitions between ATO and NATO*

There are two wings of yellow-colored surfaces in Fig. 1. Within the same LR- or RL-topologically ordered phases, ATO and NATO phases are separated by a yellow-colored surface on which the triplet gap Δ_{t} defined in Eq. (3.31b) vanishes (namely, $|\Phi_-| = |m_{\text{t}}|$). As a demonstration, we plot in Fig. 2 the blue curves by fixing $(\lambda, \widetilde{\lambda}) = (7, 1)$ in Fig. 1. In Figs. 2(a) and 2(b), we find a continuous dependence on m_{t} of the stable solution Φ_+ and Φ_- to the saddle-point equations (3.29). It follows from Eq. (3.31) that the singlet gap Δ_{s} and the triplet gap Δ_{t} in Figs. 2(c) and 2(d) are also continuous dependent on m_{t}. Moreover, the triplet gap vanishes at $|m_{\text{t}}|/\Lambda_x \approx 0.76$ that signals a continuous quantum phase transition.

The two yellow wings to the left and right of the quadrant $\lambda = \tilde{\lambda}$ in Fig. 1 are connected by a stripe (colored in brown) that separates the ATO from the NATO phases by a discontinuous quantum phase transition. As a demonstration, in the red curves of Fig. 2, we move away from $(\lambda, \widetilde{\lambda}) = (4, 4)$ in Fig. 1 by choosing $(\lambda, \widetilde{\lambda}) = 4\sqrt{2}(\sin\theta, \cos\theta)$ with $\theta = 23\pi/90$. We present the stable solution Φ_+ and Φ_- as a function of m_{t} in the red curves of Figs. 2(a) and 2(b), respectively. There is a discontinuous dependence on m_{t} of the stable solution Φ_+ and Φ_- to the saddle-point equations (3.29) that delivers a discontinuous dependence on m_{t} of the singlet gap Δ_{s} and the triplet gap Δ_{t} in the red curves of Figs. 2(c) and 2(d).

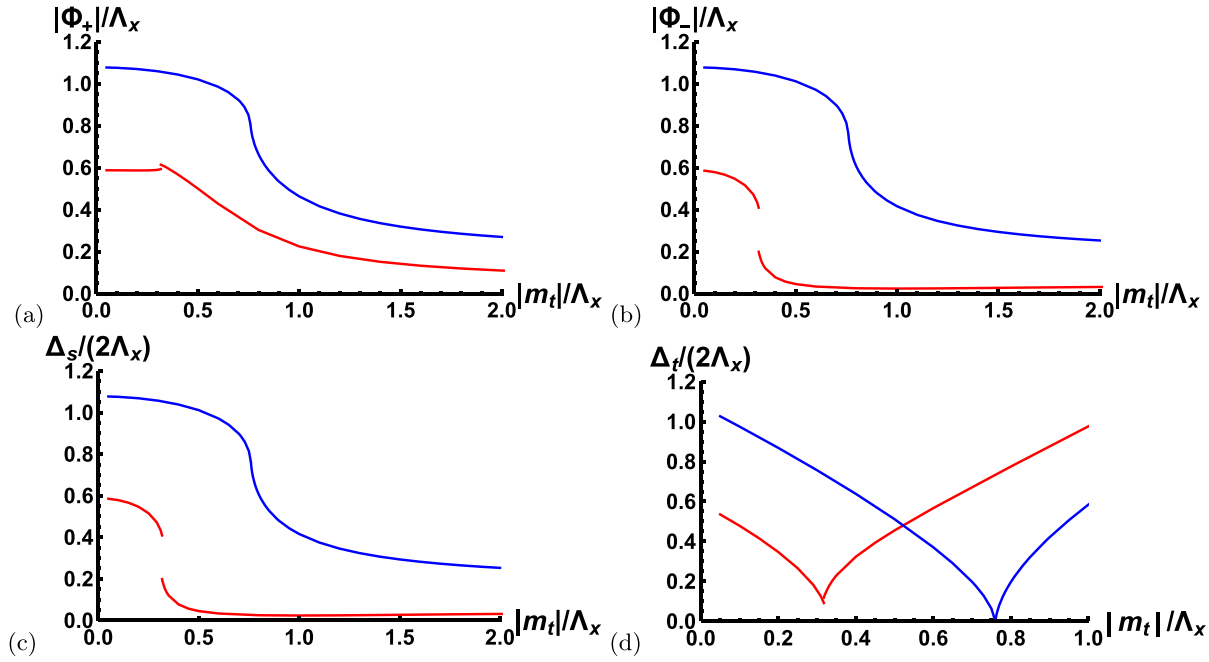

FIG. 2. Blue curve: We fix $(\lambda, \widetilde{\lambda}) = (7, 1)$ in Fig. 1 so as to strongly break time-reversal symmetry. Red curve: We fix $(\lambda, \widetilde{\lambda}) = 4\sqrt{2}(\sin\theta, \cos\theta)$ with $\theta = 23\pi/90$ in Fig. 1 so as to weakly break time-reversal symmetry. (a) and (b) Continuous and discontinuous dependences on m_t of the stable solution Φ_+ and Φ_- to the saddle-point equations (3.29). (c) and (d) Continuous and discontinuous dependences on m_t of the singlet gap Δ_s and the triplet gap Δ_t given by Eq. (3.31). The triplet gap Δ_t represented by the blue curve vanishes at $|m_t|/\Lambda_x \approx 0.76$ that signals a continuous quantum phase transition.

2. *Case* $\lambda = \tilde{\lambda}$

Figure 1(b) summarizes the numerical search for the stable solutions to the saddle-point equations (3.29) in the quadrant $\lambda = \widetilde{\lambda} \geqslant 0$ and $|m_t| \geqslant 0$, holding v_μ and m_s fixed to the values $v_\mu \equiv 1$ and $m_s = 0$, respectively. We found three distinct mean-field phases whose boundaries are shown in Fig. 1(b). One phase is gapless. Two phases are gapful when periodic boundary conditions are imposed [30]. The region bounded by the vertical axis and the green curve supports a stable solution to the saddle-point equations (3.29) with $\Phi_+ \neq 0$, but

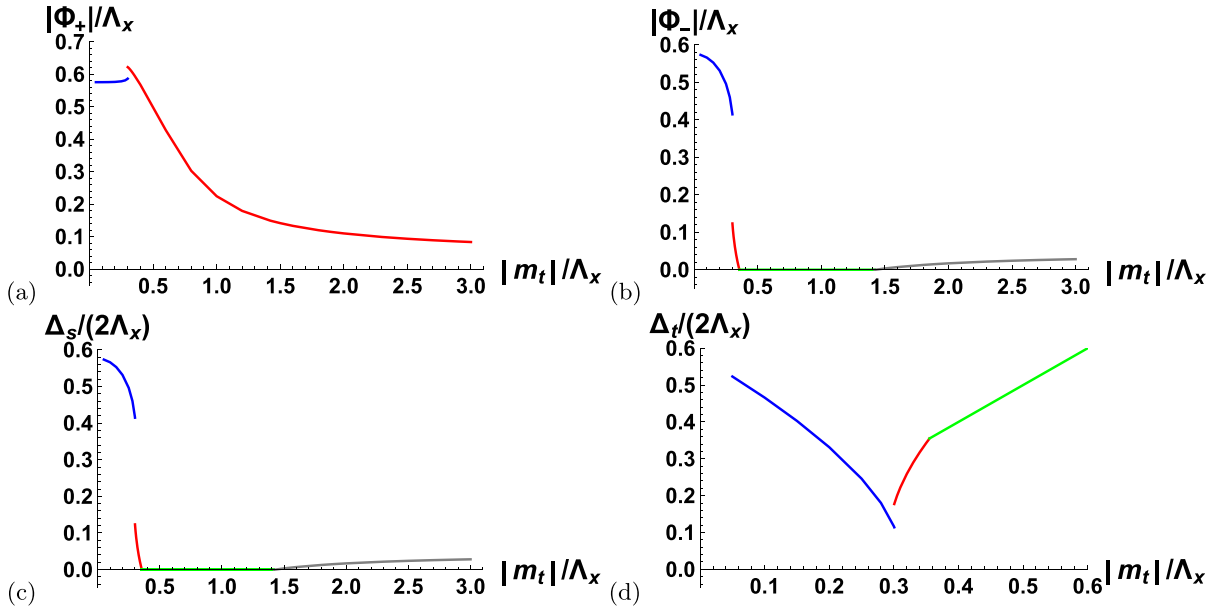

FIG. 3. (a) and (b) Cut with fixed $\lambda = \widetilde{\lambda} = 4$ from Fig. 1(b). The stable mean-field solutions Φ_+ and Φ_- are presented in panels (a) and (b) as functions of $|m_t|/\Lambda_x$, respectively. The $|m_t|/\Lambda_x$ dependence of the singlet (Δ_s) and the triplet (Δ_t) gaps are plotted in panels (c) and (d) by making use of Eqs. (3.31a) and (3.31b), respectively.

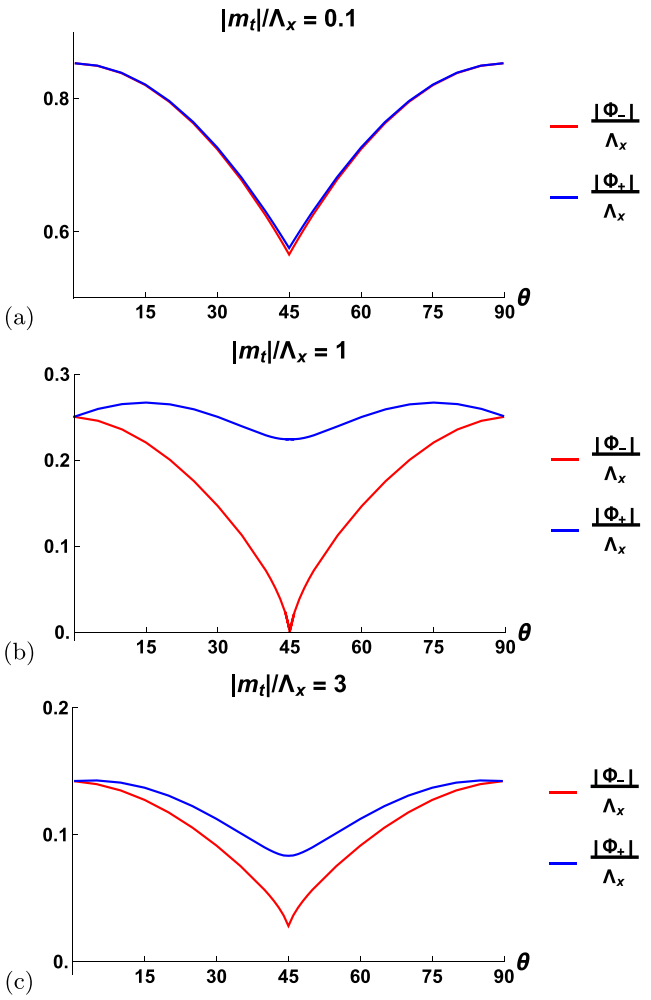

FIG. 4. The stable mean-field solutions Φ_+ and Φ_- as a function of $\theta := \arctan(\lambda/\widetilde{\lambda})$ and fixing $\lambda^2 + \widetilde{\lambda}^2 = 32$. When $\theta = \pi/4$, there is a discontinuous (respectively, continuous) phase transition for panels (a) and (c) [respectively, (b)]. (a) Case $|m_t|/\Lambda_x = 0.1$. Here, $|\Phi_+| \neq |\Phi_-|$ whereas, $||\Phi_+| - |\Phi_-|| \ll 1$. (b) Case $|m_t|/\Lambda_x = 1$. (c) Case $|m_t|/\Lambda_x = 3$.

$\Phi_- = 0$. Hence, this solution respects the time-reversal symmetry of the mean-field Hamiltonian. It follows from Eq. (3.31) that the triplet gap Δ_t is nonvanishing whereas the singlet gap Δ_s is vanishing. The triplet of the Majorana is thus gapped, whereas the singlet of the Majorana is gapless because of a Dirac-like band touching. The dashed line (colored in brown) in Fig. 1(b) is a line of discontinuous quantum phase transitions by which $|\Phi_-| < |m_t|$ above the dashed line, whereas $|\Phi_-| > |m_t|$ below the dashed line. The discontinuous jump of $|\Phi_-|$ is evidence for a mean-field discontinuous quantum phase transition. This discontinuity is mirrored in the discontinuities of Φ_+, Δ_s, and Δ_t as exemplified in Fig. 3 for $(\lambda, \tilde{\lambda}) = (4, 4)$.

As a comparison, we plot in Fig. 4 the stable mean-field solutions Φ_+ and Φ_- as a function of $\theta := \arctan(\lambda/\widetilde{\lambda})$ and fixing $\lambda^2 + \widetilde{\lambda}^2 = 32$ for $|m_t|/\Lambda_x = 0.1$, 1, and 3 in Figs. 4(a)–4(c), respectively. When $\theta = \pi/4$, there is a discontinuous (respectively, continuous) phase transition for panels (a) and (c) [respectively, (b)]. We note that, in Fig. 4(a), the value of $|\Phi_-|$ is not equal to $|\Phi_+|$ whereas $||\Phi_+| - |\Phi_-|| \ll 1$.

IV. LATTICE REGULARIZATION

We are going to show that the one-dimensional lattice model (4.1) regularizes the $(1+1)$-dimensional quantum field theory with the Hamiltonian density obtained by adding Eq. (2.1a) to Eq. (2.2) with $n = 1$. This will be achieved using the density-matrix renormalization group (DMRG) [31,32] to match quantum criticality in the quantum field theory with that in the lattice model.

We will then couple a one-dimensional array of spin-1/2 ladders of the form (4.1) as is performed in Hamiltonian (4.5) and argue that this two-dimensional lattice model regularizes the Hamiltonian density (2.4).

A. Numerical study of a two-leg ladder

Following Ref. [15], we define a spin-1/2 ladder by the Hamiltonian,

$$\begin{aligned}\widehat{H}_{\text{ladder}} := &\sum_{i=1}^{N-1} J_1 \widehat{\boldsymbol{S}}_i \cdot \widehat{\boldsymbol{S}}_{i+1} + \sum_{i'=1}^{N-1} J_1 \widehat{\boldsymbol{S}}'_{i'} \cdot \widehat{\boldsymbol{S}}'_{i'+1} + \sum_{i=1}^{N} J_\perp \widehat{\boldsymbol{S}}_i \cdot \widehat{\boldsymbol{S}}'_i \\ &+ \sum_{i=1}^{N-1} J_\times (\widehat{\boldsymbol{S}}_i \cdot \widehat{\boldsymbol{S}}'_{i+1} + \widehat{\boldsymbol{S}}_{i+1} \cdot \widehat{\boldsymbol{S}}'_i) \\ &+ \sum_{i=1}^{N-1} J_U (\widehat{\boldsymbol{S}}_i \cdot \widehat{\boldsymbol{S}}_{i+1})(\widehat{\boldsymbol{S}}'_i \cdot \widehat{\boldsymbol{S}}'_{i+1}). \end{aligned} \tag{4.1}$$

Here, $\widehat{\boldsymbol{S}}_i$ and $\widehat{\boldsymbol{S}}'_{i'}$ are spin-1/2 operators localized on the sites of the first and second legs of the ladder, respectively. There are three independent couplings obeying $J_1 > 0$ and $J_\perp, J_\times, J_U \in \mathbb{R}$ with the condition $J_\times \equiv -J_\perp/2$. References [15,33,34] have shown that, at the level of bosonization, the low-energy limit of the ladder (4.1) is the single copy ($n = 1$) of the noninteracting massive Majorana field theory defined by adding the Hamiltonian densities (2.1a) and (2.2) with the mass terms m_s and m_t related to the microscopic couplings in Eq. (4.1) by

$$m_s = \frac{-1}{2\pi}(12J_\perp + J_U), \quad m_t = \frac{1}{2\pi}(4J_\perp - J_U). \tag{4.2}$$

Bosonization thus predicts the existence for the spin-1/2 ladder (4.1) of a quantum critical point in the Ising universality class for which $m_s = 0$ as the dimensionless ratio $J_U/J_\perp$ smoothly crosses the critical value of $(J_U/J_\perp)_c \approx -1/12$. We are going to use the technique of the DMRG [31,32] to verify this prediction. We fix the units of energy by setting $J_1 = 1$, bound from above the bond dimension in the DMRG by 1500 and impose open boundary condition.

The phase diagram as a function of $J_U < 0$ and $|J_\perp| \leqslant 0.3$ is shown in Fig. 5(a). Here, CD and RS stand for columnar dimer and rung singlet, respectively. A classical representation for the CD and the RS phases is obtained by coloring nearest-neighbor bonds as shown in Figs. 5(b) and 5(c). The acronym H stands for the Haldane phase of the antiferromagnetic quantum spin-1 Heisenberg chain [35,36]. The Haldane phase is obtained when $J_\perp$ is ferromagnetic ($J_\perp < 0$) and $|J_U|$

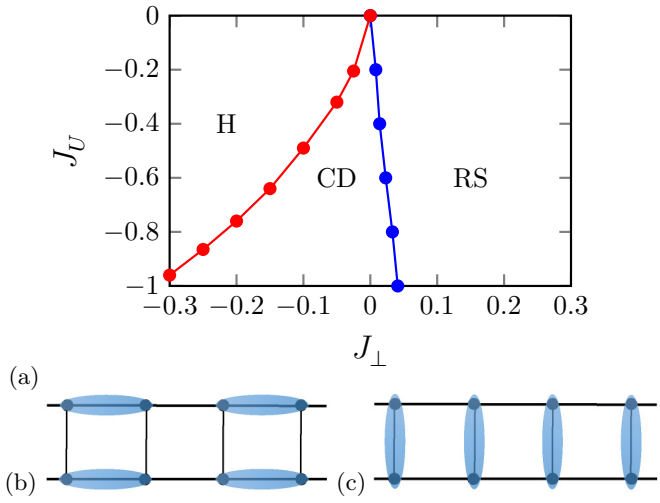

FIG. 5. (a) The phase diagram for the ladder model (4.1) as a function of $J_U < 0$ and $|J_\perp| \leqslant 0.3$. The phase boundary between the columnar-dimer (CD) and the rung-singlet (RS) phases is a continuous phase transition in the Ising universality class. The phase boundary between the Haldane phase (H) and the columnar-dimer phase is a continuous phase transition in the $\widehat{su}(2)_2$ Wess-Zumino-Novikov-Witten (WZNW) universality class. (b) Classical representation for the CD order. (c) Classical representation for the RS order.

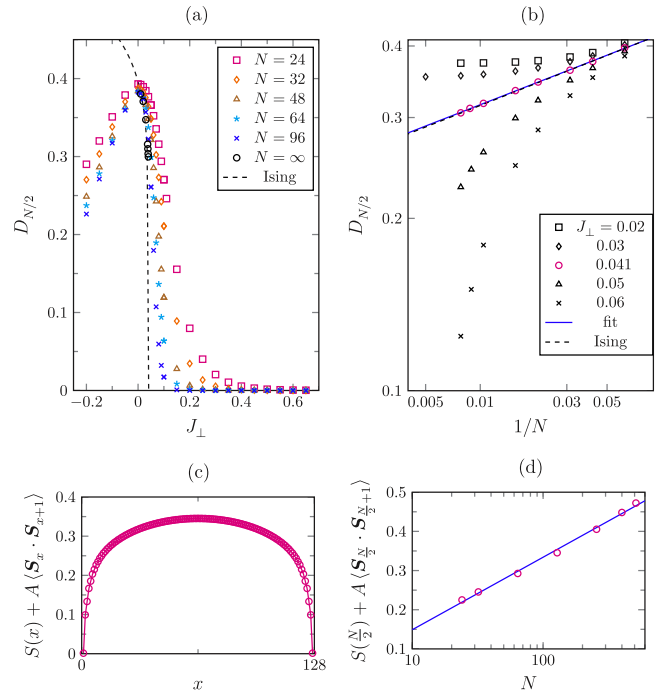

FIG. 6. (a) Plot for the leg-dimer order parameter (4.3) at the center of the ladder $D_{N/2}$ as a function of $J_\perp$ for different system sizes while fixing $J_U = -1$. The extrapolation to the thermodynamic limit is obtained with a second-order polynomial in $1/N$, whereas the dashed curve is a fit to the Ising scaling law $D_\infty(J_\perp) \propto (J_{\perp,c} - J_\perp)^{1/8}$ in the vicinity of the critical point $J_{\perp,c} \approx 0.041$. (b) Fixing $J_U = -1$, this log-log plot shows the scaling of $D_{N/2}$ with $1/N$ for different values of $J_\perp$ in the vicinity of the critical point. The Ising scaling law $D_{N/2}(J_{\perp,c}) \propto N^{-1/8}$ fits pretty well the scaling of $D_{N/2}$ at the transition point $J_{\perp,c} \approx 0.041$. (c) and (d) Fitting the entanglement entropy from Eq. (4.4) as a function of x with $N = 128$ in panel (c) and of N with $x = N/2$ in panel (d) yields $c = 0.4692$ and $c = 0.4824$, respectively.

is not too large. Increasing $|J_U|$ weakens the Haldane phase until it gives way to the CD phase. Destroying the CD phase is achieved by changing the sign of $J_\perp$ holding $|J_U|$ fixed.

The phase boundary between the CD phase and the RS phase is a continuous phase transition belonging to the two-dimensional Ising universality class. The numerical evidence for this Ising transition is supported by the finite-size scaling of the leg-dimer order parameter [14,37],

$$D_i := \langle \widehat{\boldsymbol{S}}_i \cdot (\widehat{\boldsymbol{S}}_{i+1} - \widehat{\boldsymbol{S}}_{i-1})\rangle, \quad i = 1, \ldots, N-1 \tag{4.3}$$

combined with an estimate of the central charge from the scaling of the entanglement entropy.

In Figs. 6(a) and 6(b), we fix $J_U = -1$. We then calculate $D_{N/2}(J_\perp)$ for various values of $J_\perp$ and N. We find an Ising critical point at $J_{\perp,c} \approx 0.041$ for which the Ising scaling laws [37] for the order parameter provide an excellent fit.

Another piece of evidence to support the Ising transition is provided by the scaling form of the bipartite von Neumann entanglement entropy under an open boundary condition [37–42]. It is given by

$$S(x, N) = \frac{c}{6} \ln\left(\frac{N+1}{\pi} \sin\frac{\pi x}{N+1}\right) + A\langle \widehat{\boldsymbol{S}}_x \cdot \widehat{\boldsymbol{S}}_{x+1}\rangle + B. \tag{4.4}$$

Here, x is the position of the rung at which we partition the ladder into left and right "worlds," c is the (to be determined) central charge, and A, B are nonuniversal constants. In Figs. 6(c) and 6(d), we fix $J_U = -1$ and $J_\perp = 0.041$. In Fig. 6(c), we vary x keeping N fixed. In Fig. 6(d), we fix $x = N/2$ and vary N. Both calculations are consistent with an Ising transition for which the exact central charge $c = 1/2$.

The phase boundary between the H phase and the RS phase in Fig. 5(a) is predicted within the bosonization framework to be a continuous phase transition belonging to the $(1+1)$-dimensional $\widehat{su}(2)_2$ WZNW universality class. The central charge is $3/2$, and the critical exponent for the scaling of the order parameter is $3/8$. We have obtained DMRG evidence for such a transition in the same way as was performed for the Ising transition. As this transition is not the focus of this paper, we will not present these numerical results.

We conclude this section by observing that the spin ladder model defined in Eq. (4.1) with $J_\times \equiv 0$ was recently studied in Ref. [43]. Reference [43] derives a phase diagram similar to that shown in Fig. 5(a). The only differences are the slopes of the phase boundaries. These differences can be understood from the fact that the phase boundaries of the spin-1/2 ladder (4.1) are determined by the zeros of the masses of the Majorana fields (4.2). Choosing different intraladder couplings changes the relation (4.2) between the masses of the Majorana fields and the microscopic couplings. This change affects the slopes of the phase boundaries in the microscopic model. We opted to introduce a nonvanishing coupling $J_\times \equiv -J_\perp/2$ in Hamiltonian (4.1) in order to suppress all the bare couplings for all marginally relevant perturbations to the $\widehat{su}(2)_1 \oplus \widehat{su}(2)_1$ WZWN critical point [i.e., all couplings except J_1 set to zero in Eq. (4.1)] [15,33].

B. Model of coupled spin-1/2 two-leg ladders

We take n copies labeled by the index $\mathrm{m} = 1, \ldots, n$ of the spin-1/2 ladder (4.1). We couple this array of spin-1/2 ladders with the interladder interaction [15],

$$\widehat{H}_{\text{interladder}} := \widehat{H}_{\triangle} + \widehat{H}'_{\triangle} + \widehat{H}_{\square} + \widehat{H}'_{\square}, \tag{4.5a}$$

where

$$\widehat{H}_{\triangle} := \frac{J_\chi}{2} \sum_{\mathrm{i}=1}^{N} \sum_{\mathrm{m}=1}^{\mathrm{n}-1} \big[\widehat{\boldsymbol{S}}_{\mathrm{i,m+1}} \cdot (\widehat{\boldsymbol{S}}_{\mathrm{i+1,m}} \wedge \widehat{\boldsymbol{S}}_{\mathrm{i,m}}) + \widehat{\boldsymbol{S}}_{\mathrm{i+1,m}} \cdot (\widehat{\boldsymbol{S}}_{\mathrm{i,m+1}} \wedge \widehat{\boldsymbol{S}}_{\mathrm{i+1,m+1}}) \big], \tag{4.5b}$$

and

$$\widehat{H}_{\square} := J_\vee \sum_{\mathrm{i}=1}^{N} \sum_{\mathrm{m}=1}^{n-1} \Big(\widehat{\boldsymbol{S}}_{\mathrm{i,m}} \cdot \widehat{\boldsymbol{S}}_{\mathrm{i,m+1}} + \frac{1}{2} \widehat{\boldsymbol{S}}_{\mathrm{i,m+1}} \cdot \widehat{\boldsymbol{S}}_{\mathrm{i+1,m}} + \frac{1}{2} \widehat{\boldsymbol{S}}_{\mathrm{i,m}} \cdot \widehat{\boldsymbol{S}}_{\mathrm{i+1,m+1}} \Big), \tag{4.5c}$$

with $\widehat{H}'_{\triangle}$ and $\widehat{H}'_{\square}$ deduced from $\widehat{H}_{\triangle}$ and $\widehat{H}_{\square}$ by the substitution $\widehat{\boldsymbol{S}}_{\mathrm{i,m}} \to \widehat{\boldsymbol{S}}'_{\mathrm{i,m}}$. The low-energy limit of Hamiltonian $\widehat{H}_{\text{interladder}}$ was obtained using bosonization in Refs. [14,15] (see also Ref. [11]). Aside from a renormalization of the velocities entering the quadratic Hamiltonian density (2.1a), it produces as was shown in Ref. [44] the quartic Majorana interaction (2.3) with the couplings λ and $\widetilde{\lambda}$ related to the microscopic couplings entering Eq. (4.5b) by [14,15]

$$\lambda = 2\mathfrak{a}[(J_\chi/\pi) + 2J_\vee], \quad \widetilde{\lambda} = 2\mathfrak{a}[-(J_\chi/\pi) + 2J_\vee]. \tag{4.6a}$$

We will use shortly the reciprocal relation,

$$J_\vee = \frac{1}{8\mathfrak{a}}(\lambda + \widetilde{\lambda}), \quad J_\chi = \frac{\pi}{4\mathfrak{a}}(\lambda - \widetilde{\lambda}). \tag{4.6b}$$

The two-dimensional spin-1/2 model is then defined by

$$\widehat{H} := \widehat{H}^{\text{array}}_{\text{ladder}} + \widehat{H}_{\text{interladder}}, \tag{4.7}$$

where $\widehat{H}^{\text{array}}_{\text{ladder}}$ is simply the sum of n copies of the spin-1/2 ladder (4.1).

C. Implications

We are now ready to deduce from the mean-field phase diagram Fig. 1 of the quantum field theory (2.4) the following predictions for the two-dimensional array of coupled spin-1/2 ladders (4.7).

First, fixing $m_{\mathrm{s}} = 0$ implies the linear condition [cf. Eq. (4.2)],

$$J_\perp \propto -J_U. \tag{4.8}$$

It then follows that m_{t} is only controlled by one parameter, namely,

$$|m_{\mathrm{t}}| \propto |J_\perp| \propto |J_U|. \tag{4.9}$$

Second, fixing $\lambda = \widetilde{\lambda}$ implies $J_\chi \equiv 0$, i.e., the three-spin interaction that breaks explicitly time-reversal symmetry must vanish. We then deduce from the quantum field theory (2.4) that the two-dimensional spin-1/2 lattice model (4.7) could support three phases of which two are gapped and break spontaneously the time-reversal symmetry whereas one is gapless and time-reversal symmetric. There is an important caveat here, namely, that we have neglected perturbations, whose bare couplings are very small (e.g., generated by quantum corrections) but relevant at the $\bigoplus_{\mathrm{m}}[\widehat{su}(2)_1 \oplus \widehat{su}(2)_1]$ WZWN critical point that would stabilize the collinear long-ranged ordered phase or dimer phases [45,46]. If we ignore this possibility, a too small or too large $|m_{\mathrm{t}}| \propto |J_\perp| \propto |J_U|$ could then stabilize a topologically ordered spin-liquid phase, whereas intermediate values of $|m_{\mathrm{t}}| \propto |J_\perp| \propto |J_U|$ with $\lambda = \widetilde{\lambda} \propto J_\vee > 0$ not too large (say, $\lambda \lesssim 8$) could stabilize a gapless spin-liquid phase with a Dirac point. The mean-field transition through the time-reversal-symmetric quadrant $\lambda = \widetilde{\lambda}$ from the region with $\lambda < \widetilde{\lambda}$ to the region with $\lambda > \widetilde{\lambda}$ is continuous (discontinuous) if it goes through the gapless (one of the gapped) phase.

V. SUMMARY

We have studied a strongly interacting QFT describing a two-dimensional array of wires containing four (a singlet and a triplet) massive Majorana fields in $(1+1)$-dimensional space-time. This QFT is a continuum limit of a two-dimensional lattice model of spins $S = 1/2$ interacting via $SU(2)$ symmetric two-, three-, and four-spin interactions. In the continuum limit, these interactions give rise to two Majorana masses and to competing quartic Majorana interactions (with couplings λ and $\widetilde{\lambda}$) that are interchanged under time reversal. The case of $\lambda \neq 0$, $\widetilde{\lambda} = 0$ when the time reversal is explicitly broken was studied by us before [15]. Here, we have considered the limit $\lambda = \widetilde{\lambda}$ and established the conditions under which time-reversal symmetry is broken spontaneously.

At the mean-field level on the time-reversal-symmetric plane $\lambda = \widetilde{\lambda}$, we have found three competing phases. There are two gapped phases that break spontaneously the time-reversal symmetry; they are gapped in the bulk and support chiral Majorana edge modes carrying the chiral central charges 2 and 1/2, respectively. One phase is conjectured to signal an ATO; the other is conjectured to signal a NATO if the mean-field approximation is relaxed. This pair of mean-field gapped phases is separated by a line of points at which a discontinuous phase transition takes place. However, we have also found a time-reversal-symmetric mean-field phase that supports a branch of mean-field Majorana modes with a gapless Dirac spectrum. This phase is bounded by a line of continuous phase transitions separating it from the mean-field snapshot of the NATO phase.

We remark that, although we have assumed that the singlet mass m_{s} is vanishing in our mean-field analysis and treated the triplet mass m_{t} as a tunable parameter, we could equally well have reversed the roles of the singlet and triplet masses. If so, we can simply exchange the role played by the triplet and the singlet Majorana modes. The resulting mean-field phase diagram would contain again the mean-field snapshots of an Abelian phase and of a non-Abelian phase. The Abelian phase is the same Abelian phase as in the present paper. The non-Abelian phase would be different, however, as its chiral edge modes would carry a chiral central charge of 3/2. A non-Abelian topologically ordered phase with chiral edge states endowed with the central charge 3/2 is a cousin to

the Moore-Read state for the fractional quantum Hall effect [4]. One also finds such a non-Abelian topologically ordered phase for certain spin-1 Heisenberg models on the square lattice [47].

ACKNOWLEDGMENTS

The DMRG calculations were performed using the ITensor library [48] on the Euler cluster at ETH Zürich, Switzerland. J.-H.C. was supported by the Swiss National Science Foundation (SNSF) under Grant No. 2000021 153648. C.C. was supported by the U.S. Department of Energy (DOE), Division of Condensed Matter Physics and Materials Science, under Contract No. DE-FG02-06ER46316. A.M.T. was supported by the U.S. Department of Energy, Office of Basic Energy Sciences, under Contract No. DE-SC0012704. C.C. acknowledges the hospitality of the Pauli Center for Theoretical Studies at ETH Zürich and the University of Zürich.

[1] V. Kalmeyer and R. B. Laughlin, Equivalence of the Resonating-Valence-Bond and Fractional Quantum Hall States, Phys. Rev. Lett. **59**, 2095 (1987).
[2] X.-G. Wen, Topological orders and chern-simons theory in strongly correlated quantum liquid, Int. J. Mod. Phys. B **05**, 1641 (1991).
[3] A. Kitaev, Anyons in an exactly solved model and beyond, Ann. Phys. (N. Y.) **321**, 2 (2006).
[4] G. Moore and N. Read, Nonabelions in the fractional quantum hall effect, Nucl. Phys. B **360**, 362 (1991).
[5] R. Mukhopadhyay, C. L. Kane, and T. C. Lubensky, Crossed sliding luttinger liquid phase, Phys. Rev. B **63**, 081103(R) (2001).
[6] C. L. Kane, R. Mukhopadhyay, and T. C. Lubensky, Fractional Quantum Hall Effect in an Array of Quantum Wires, Phys. Rev. Lett. **88**, 036401 (2002).
[7] J. C. Y. Teo and C. L. Kane, From luttinger liquid to non-abelian quantum hall states, Phys. Rev. B **89**, 085101 (2014).
[8] C. L. Kane, A. Stern, and B. I. Halperin, Pairing in Luttinger Liquids and Quantum Hall States, Phys. Rev. X **7**, 031009 (2017).
[9] C. L. Kane and A. Stern, Coupled wire model of Z_4 orbifold quantum hall states, Phys. Rev. B **98**, 085302 (2018).
[10] X. G. Wen, Chiral luttinger liquid and the edge excitations in the fractional quantum hall states, Phys. Rev. B **41**, 12838 (1990).
[11] G. Gorohovsky, R. G. Pereira, and E. Sela, Chiral spin liquids in arrays of spin chains, Phys. Rev. B **91**, 245139 (2015).
[12] P.-H. Huang, J.-H. Chen, P. R. S. Gomes, T. Neupert, C. Chamon, and C. Mudry, Non-abelian topological spin liquids from arrays of quantum wires or spin chains, Phys. Rev. B **93**, 205123 (2016).
[13] P. Lecheminant and A. M. Tsvelik, Lattice spin models for non-abelian chiral spin liquids, Phys. Rev. B **95**, 140406(R) (2017).
[14] P.-H. Huang, J.-H. Chen, A. E. Feiguin, C. Chamon, and C. Mudry, Coupled spin-$\frac{1}{2}$ ladders as microscopic models for non-abelian chiral spin liquids, Phys. Rev. B **95**, 144413 (2017).
[15] J.-H. Chen, C. Mudry, C. Chamon, and A. M. Tsvelik, Model of chiral spin liquids with abelian and non-abelian topological phases, Phys. Rev. B **96**, 224420 (2017).
[16] R. G. Pereira and S. Bieri, Gapless chiral spin liquid from coupled chains on the kagome lattice, Sci. Post. Phys. **4**, 004 (2018).
[17] X. G. Wen, F. Wilczek, and A. Zee, Chiral spin states and superconductivity, Phys. Rev. B **39**, 11413 (1989).
[18] N. Read and D. Green, Paired states of fermions in two dimensions with breaking of parity and time-reversal symmetries and the fractional quantum hall effect, Phys. Rev. B **61**, 10267 (2000).
[19] D. A. Ivanov, Non-abelian Statistics of Half-Quantum Vortices in p-Wave Superconductors, Phys. Rev. Lett. **86**, 268 (2001).
[20] J. Nasu, Y. Kato, Y. Kamiya, and Y. Motome, Successive majorana topological transitions driven by a magnetic field in the kitaev model, Phys. Rev. B **98**, 060416(R) (2018).
[21] G. Jackeli and G. Khaliullin, Mott Insulators in the Strong Spin-Orbit Coupling Limit: From Heisenberg to a Quantum Compass and Kitaev Models, Phys. Rev. Lett. **102**, 017205 (2009).
[22] M. Hermanns, I. Kimchi, and J. Knolle, Physics of the Kitaev model: Fractionalization, dynamic correlations, and material connections, Annu. Rev. Condens. Matter Phys. **9**, 17 (2018).
[23] The lattice model that underlies the phase diagram (see Fig. 1) is shared with that of the magnetic ions in the material $BiCu_2PO_6$ [49]. However, the compound $BiCu_2PO_6$ does not realize a quantum spin liquid .
[24] F. F. Assaad and T. Grover, Simple Fermionic Model of Deconfined Phases and Phase Transitions, Phys. Rev. X **6**, 041049 (2016).
[25] F. D. M. Haldane, Model for a Quantum Hall Effect Without Landau Levels: Condensed-Matter Realization of the "Parity Anomaly", Phys. Rev. Lett. **61**, 2015 (1988).
[26] A. M. Tsvelik, *Quantum Field Theory in Condensed Matter Physics* (Cambridge University Press, Cambridge, U.K., 2003).
[27] In Eq. (3.24b), the integral over ω can be carried out by using the following formula for a definite integral [50]:

$$\int_{-\infty}^{\infty} \frac{d\omega}{2\pi} \ln(\omega^2 + k^2 + A^2) = \sqrt{k^2 + A^2} + \text{const},$$

where the constant is formally infinity.
[28] J. Fröhlich and F. Gabbiani, Braid statistics in local quantum theory, Rev. Math. Phys. **02**, 251 (1990).
[29] K. H. Rehren, in *The Algebraic Theory of Superselection Sectors. Introduction and Recent Results*, edited by D. Kastler (World Scientific, Singapore, 1990), p. 333.
[30] On one hand, *periodic boundary conditions* were imposed in order to compute the bulk spectrum [cf. Eq. (3.7) and thereafter]. On the other hand, the existence of gapless edge states requires *open boundary conditions*.
[31] S. R. White, Density Matrix Formulation for Quantum Renormalization Groups, Phys. Rev. Lett. **69**, 2863 (1992).
[32] S. R. White, Density-matrix algorithms for quantum renormalization groups, Phys. Rev. B **48**, 10345 (1993).
[33] D. G. Shelton, A. A. Nersesyan, and A. M. Tsvelik, Antiferromagnetic spin ladders: Crossover between spin $S = 1/2$ and $S = 1$ chains, Phys. Rev. B **53**, 8521 (1996).

[34] A. A. Nersesyan and A. M. Tsvelik, One-Dimensional Spin-Liquid Without Magnon Excitations, Phys. Rev. Lett. **78**, 3939 (1997).

[35] F. D. M. Haldane, Continuum dynamics of the 1-D heisenberg antiferromagnet: Identification with the O(3) nonlinear sigma model, Phys. Lett. A **93**, 464 (1983).

[36] F. D. M. Haldane, Nonlinear Field Theory of Large-Spin Heisenberg Antiferromagnets: Semiclassically Quantized Solitons of the One-Dimensional Easy-Axis Néel State, Phys. Rev. Lett. **50**, 1153 (1983).

[37] A. Lavarélo, G. Roux, and N. Laflorencie, Melting of a frustration-induced dimer crystal and incommensurability in the J_1-J_2 two-leg ladder, Phys. Rev. B **84**, 144407 (2011).

[38] P. Calabrese and J. Cardy, Entanglement entropy and quantum field theory, J. Stat. Mech.: Theory Exp. (2004) P06002.

[39] P. Calabrese and J. Cardy, Entanglement entropy and conformal field theory, J. Phys. A: Math. Theor. **42**, 504005 (2009).

[40] N. Laflorencie, E. S. Sørensen, M.-S. Chang, and I. Affleck, Boundary Effects in the Critical Scaling of Entanglement Entropy in 1D Systems, Phys. Rev. Lett. **96**, 100603 (2006).

[41] I. Affleck, N. Laflorencie, and E. S. Sørensen, Entanglement entropy in quantum impurity systems and systems with boundaries, J. Phys. A: Math. Theor. **42**, 504009 (2009).

[42] J. Cardy and P. Calabrese, Unusual corrections to scaling in entanglement entropy, J. Stat. Mech.: Theory Exp. (2010) P04023.

[43] N. J. Robinson, A. Altland, R. Egger, N. M. Gergs, W. Li, D. Schuricht, A. M. Tsvelik, A. Weichselbaum, and R. M. Konik, Nontopological Majorana Zero Modes in Inhomogeneous Spin Ladders, Phys. Rev. Lett. **122**, 027201 (2019).

[44] A. M. Tsvelik, Field-theory treatment of the heisenberg spin-1 chain, Phys. Rev. B **42**, 10499 (1990).

[45] O. A. Starykh and L. Balents, Dimerized Phase and Transitions in a Spatially Anisotropic Square Lattice Antiferromagnet, Phys. Rev. Lett. **93**, 127202 (2004).

[46] O. A. Starykh and L. Balents, Ordering in Spatially Anisotropic Triangular Antiferromagnets, Phys. Rev. Lett. **98**, 077205 (2007).

[47] J.-Y. Chen, L. Vanderstraeten, S. Capponi, and D. Poilblanc, Non-abelian chiral spin liquid in a quantum antiferromagnet revealed by an ipeps study, Phys. Rev. B **98**, 184409 (2018).

[48] ITensor library (version 2.1.1), https://itensor.org/.

[49] F. Casola, T. Shiroka, A. Feiguin, S. Wang, M. S. Grbić, M. Horvatić, S. Krämer, S. Mukhopadhyay, K. Conder, C. Berthier, H.-R. Ott, H. M. Rønnow, C. Rüegg, and J. Mesot, Field-Induced Quantum Soliton Lattice in a Frustrated Two-Leg Spin-1/2 Ladder, Phys. Rev. Lett. **110**, 187201 (2013).

[50] M. Stone, *The Physics of Quantum Fields* (Springer, New York, 2000).